A two-dimensional population balance model for cell growth including multiple uptake systems

V. Quedeville, H. Ouazaite, Bastien Polizzi, R.O. Fox, P. Villedieu, Pascal Fede, F. Létisse, J. Morchain

A two-dimensional population balance model for cell growth including multiple uptake systems

V. Quedeville[b,a], H. Ouazaite[a], B. Polizzi[b], R.O. Fox[c], P. Villedieu[d,a], P. Fede[b], F. Létisse[a], J. Morchain[a,*]

[a] Laboratoire d'Ingénierie des Systèmes biologiques et des Procédés, INSA de Toulouse, 135 Avenue de Rangueil, 31400 Toulouse, France
[b] Institut de Mécanique des Fluides de Toulouse, 2 Allée du professeur Camille Soula, 31000 Toulouse, France
[c] Department of Chemical and Biological Engineering, Iowa State University, 618 Bissell Road, Ames, IA 50011-1098, United States
[d] ONERA de Toulouse, 2 Avenue Edouard Belin, 31055 Toulouse, France

Keywords:
Cell growth
Population balance model
Uptake rate
Bioreactor
Dynamic simulation

Cell growth in a chemostat is a well-documented research topic. How cells uptake the available substrate to gain weight and engage cell division is not generally taken into account in the modelling bioreactors. In fact, the growth rate is related to a population doubling time whereas the microorganisms' growth in mass is due to the mass transfer of substrates from the liquid phase to the biotic phase. Clearly, growth in mass precedes growth in number. Similarly, the transport of substrates down to the cell scale precedes the mass transfer. This article's main feature is a two-dimensional population balance model that allows to uncouple growth in mass and growth in number when the equilibrium between a cell population and its environment is disrupted. The cell length and the rate of anabolism are chosen as internal variables. It is proved that the hypothesis "growth in number = growth in mass" is valid at steady-state or in exponential growth only. The glucose uptake is assumed driven by two transport systems with a different affinity constant for the substrate. This combination of two regulated uptake systems operating in parallel explains a 3-fold increase in the uptake following a glucose pulse, but can also predict substrate uptake rates higher than the maximal batch value as observed in some experiments. These features are obtained by considering carbon fluxes in the formulation of regulation principles for uptake dynamics. The population balance's implementation in a multi-compartment reactor is a natural prospective work and allows extensions to industrial processes.

1. Introduction

From a chemical-engineering perspective, aerated bioreactors have to be regarded as three-phase reactors, and the prediction of mass transfer between phases is a central issue. Given the abundance of literature pertaining to the gas–liquid aspects of the problem, this topic will be put aside here. One point specific to liquid–cell mass transfer is that there is no thermodynamic law to prescribe the relationship between the concentrations at the cell interface. Thus, in living systems, the mass-transfer intensity through the cell membrane is dynamically adjusted in order to fit the cell's needs (Ferenci, 1996). The latter can correspond to a maximum growth rate in a non-limiting environment, or be dictated by the environmental conditions such as the imposed dilution rate in a chemostat. As a consequence, in exponentially growing cultures (balanced-growth phase) and in chemostat cultures, a strict proportionality is observed between the mass-transfer rate (or uptake rate in the field of biochemical engineering) and the growth rate. Moreover the latter is correlated to the

* *Corresponding author.*
E-mail address: morchain@insa-toulouse.fr (J. Morchain).

https://doi.org/10.1016/j.cherd.2018.02.025

residual concentrations of nutrients in the liquid phase. These well-known observations led to the formulation of specific growth (μ) and uptake rates (q_S) as algebraic functions of the substrate concentration in the liquid phase:

$$\mu = f(S), \tag{1.1}$$

$$q_S = Y_{SX}(\mu)\ \mu, \tag{1.2}$$

where Y_{SX} is the average mass of substrate required to yield 1 g of cells. Note that these models are relevant to fit experimental data (they are in fact empirical correlations), and thus are limited to the situation in which they are fitted. In particular, the steady-state or balanced-growth assumption implies that they are time-averaged laws.

In light of these remarks, we could preferably use a more explicit notation for the specific growth ($\bar{\mu}$) and uptake ($\bar{q}_S$) rates:

$$\bar{\mu} = f(S) \tag{1.3}$$

$$\bar{q}_S = \frac{1}{\tau}\int_t^{t+\tau} q_S(t)\ dt \approx Y_{SX}(\bar{\mu})\ \bar{\mu}, \tag{1.4}$$

where the overbar indicates a time average. Clearly, the value of the time scale τ must be large enough so that the mean uptake rate becomes constant and proportional to the mean specific growth rate. These time-averaged quantities are relevant to describe the pseudo-steady-state dynamics, however they are not applicable to the transient response (over time scales shorter than τ) because they assume an instantaneous adaptation of the living system (Silveston et al., 2008). In view of improving the dynamical modelling of bioreactors, it is important to be able to prescribe a substrate uptake model valid on the shortest time scale possible. As far as we know, there are only a few studies dedicated to this point. Chassagnole and co-workers derived a dynamic model for the glucose uptake through the PhosphoTransferase System (PTS) (Chassagnole et al., 2002) based on a detailed description of the glycolysis and pentose-phosphate pathways. Even in its reduced form, this model involves five internal concentrations and requires a large number of parameters to be fitted. Moreover, Ferenci has identified the existence of multiple transport systems whose activity depends on the substrate concentration (Ferenci, 1996) and proposed that the uptake rate is computed as the sum of the contribution of each system (Ferenci, 1999a).

The experimental measurement of the substrate uptake rate has received much attention in the last decades. Neubauer's 1990s experimental work (Neubauer et al., 1995) revealed that the instantaneous uptake rate of *Escherichia coli* cells, cultivated in a two-compartment (Continuous Stirred Reactor + Plug Flow Reactor) bioreactor operated in fed-batch mode and subject to repeated exposures to high glucose concentrations, could largely exceed the maximum uptake rate observed in a batch reactor. The experimental device was such that the first 120 s after the exposure to a glucose pulse could be observed with a temporal resolution of 30 s. More recently, Lara et al. (2009) using a bioscope measured the instantaneous uptake rate of *E. coli* cells sampled from a continuous stirred bioreactor. Their results confirmed in both aerobic and anoxic conditions that the uptake rate in the few seconds following the addition of glucose largely exceeds the maximum uptake rate measured in batch culture (based on the definition of a substrate to biomass yield and a maximum specific growth rate). The temporal resolution here is raised up to ≈3 s and the duration of the observation limited to 90 s. These are experimental evidence that the correlation between growth, uptake and the substrate concentration established in non-limiting or steady-state conditions is not valid on very short time scales ($\tau < 10$ s) when the transient response of the uptake system is involved. The results obtained by Sunya et al. (2012) who examined the dynamic response of *E. coli* cells to glucose pulses in chemostat cultures, with a temporal resolution of ≈25 s over longer periods of time offer an opportunity to establish a closure model in the situation where $\tau \approx$ 5–30 min. Natarajan and Srienc (2000) examined the uptake of a glucose analogue at the cell level using cytometry. Their results revealed that the substrate uptake rate (after 5 min following a pulse addition) is distributed in the population of cells.

The use of the population balance concept to deal with the population dynamics has been identified as the most natural way to proceed, for some time (Fredrickson and Tsuchiya, 1963). PBMs were first introduced by Smoluchowski (1916) to model the size of particles undergoing coalescence and rupture.

In biology, PBMs are rife to describe the dynamics of a cell property (age, size, mass, intracellular concentration of an enzyme representative of the cell's state) among a population of individuals. Such modelling of biological systems was introduced by Von Forster (1959) to take into account the influence of mortality over the age of a population. The cell-cycle effect was then emphasised by Bell and Anderson (1967) under the assumption that one cell gives birth to two identical daughters. In the earliest works, 1-D PBM have been derived. Most of proposed models (Eakman et al., 1966; Subramanian et al., 1970; Shah et al., 1976), and the many papers these references have inspired, relate a cell's state to its mass or volume, which requires a formulation of other properties (such as age, growth and reaction rates, or substrate consumption for instance) as functions of the mass, which has proved insufficient and rather inconclusive (for all processes that are not related to mass in the cell functioning). Many other variables may turn out to be relevant depending on the biological behaviour of the cells under consideration. One of them is maturity, highlighted by Trucco (1965), and understood (Lebowitz and Rubinow, 1974) as the cytological age, $a_c \in [0, 1]$. This formulation yields a boundary condition that connects the number density at $a_c = 0$ and $a_c = 1$: the production of new born cells (with $a_c = 0$) equals the flux of cells reaching $a_c = 1$. A unique solution in $\mathcal{C}^0(\mathbb{R}_+, L^1(\Omega))$ (Ω once again standing for the internal variable's domain) is inferred from the initial condition.

In general, 1-D PBMs fail to provide a comprehensive perspective across different time scales. Models aimed at depicting the cell cycle (for which the internal variable may be mass, length or volume) are ill-adapted for explaining the variations in a population's total mass. On the other hand, when it comes to maturity (consequently the doubling time), all age-related information is filtered and only phenomena driven by a characteristic time equating to cell growth are reachable.

An alternative is to develop a multi-dimensional PBM that includes many cell properties like DNA concentration (Hatzis et al., 1995; Stamatakis and Zygourakis, 2010) or enzymes expression levels (Mantzaris, 2005), which has turned out to be a significant step forward regarding mathematical modelling in biology. However, the completeness of such a model is always subject to doubt, and due to the large number of internal variables they can quickly become computationally

intractable. Rotenberg (1977, 1983) gave a complete 2-D model for the cell cycle, which includes age and growth rate as internal variables. Mischler et al. (2004) extracted an eigenvector that geometrically shapes the steady-state solution and an eigenvalue (the so-called Malthus parameter) that drives the exponential steady-state growth in time. The existence and uniqueness of the solution in $\mathcal{C}^0(\mathbb{R}_+, L^1(\Omega))$ is guaranteed provided the initial condition lies in $L^1(\Omega)$ and the fragmentation function in L^∞. In other words the existence of a division phenomena at the cell level ensures that the number of cells will eventually grow exponentially with time after a transition period. This result is independent from the growth rate law rate prescribed at the cell level. Perthame's seminal work (Perthame, 2007) was enlightening regarding the L^1 exponential decay of the solution to a transport-fragmentation equation such as the cell cycle dynamics, along with bounded variation regularity, provided the breakage function lies in L^∞ on its domain.

At the end of the day, in order to have a description of both the cell-scale and population-scale behaviours, a PBM needs a minimum of two degrees of freedom. These observations argues for the development of a PBM describing the cell cycle as the result of the following steps: (i) transport of nutrients down to the cell membrane, (ii) substrate uptake, (iii) transformation into new cell constituents leading to cell elongation, and (iv) cell division.

The principal objective of this work is therefore to introduce a 2-D PBM for cell growth that allows to distinguish between growth in mass and growth in number. The present model can be regarded as an extension of a previously published 1-D model whose characteristic time scale is the inverse of the population maximum specific growth rate (Morchain et al., 2017). Introducing a second dimension allows the uncoupling of the growth in mass (related to substrate uptake) and the growth in number (related to cell division). In the first part of this paper, the 2-D model is presented along with the hypothesis and assumptions. Then some properties of the model are examined. In particular, we discuss the situations leading to the equivalence between growth in mass and growth in number. We also propose an integration of the 2-D PBM leading to a population-averaged model and we enlighten the consequences of such a simplification on the predictive capacity of the integrated model. In the third part, the issue of formulating an instantaneous uptake law is addressed. Finally, the proposed model is subjected to validation through the simulation of a pulse experiment in a chemostat for which data are available in the literature.

2. Modelling framework

2.1. *Statement of assumptions regarding the biological system*

(i) We consider in this work the case of rod-shaped cells having a constant diameter d and a varying length l. This assumption corresponds to various, widespread microorganisms such as *E. coli* (Subramanian et al., 1970) and *Schizosaccharomyces pombe* (Nobs and Maerkl, 2014). Note that the cell volume $\pi\frac{d^2}{4}l$ and surface $\pi d\, l$ are only functions of l. In this particular case, the ratio of the cell surface to the cell mass is constant $A_e = \frac{4}{\rho_c d}$ where ρ is the cell mass density.

(ii) Besides its length, each cell in the population is characterized by its elongation rate v. This rate is related to the physiological state of the microorganism and more specifically to the rate of anabolism. For a given strain, Nobs and Maerkl (2014) found that the elongation rate is cell-specific and constant throughout the cell cycle.

(iii) The cell division is driven by a size mechanism, thus the probability that a cell divides is related to its length (Robert et al., 2014). When a cell of length l divides, two daughters of approximate size $l/2$ are formed. The sum of the daughters' lengths equals that of the mother cell, which can also be regarded as a conservation of the total cell mass through cell division.

(iv) The elongation rate is redistributed at cell division, which means the two daughters may not be able to perform anabolic reactions at the same rate as their mother. If both newborn cells can thrive with an arbitrary rate of anabolism, the latter is reportedly distributed around that of the mother's. This is consistent with the fact that the cell content is not evenly distributed among the two daughters (for instance Stamatakis and Zygourakis (2010) assumed the redistribution follows a hypergeometric law).

(v) In order to grow, cells uptake a carbon source (typically glucose) and oxygen. At steady state in a chemostat or in the balanced-growth phase of a batch culture, the specific growth rate of the entire population is correlated to the concentration of the substrate in the culture medium. This correlation takes the usual Monod form:

$$\mu^\star = \mu_{\max}\frac{S}{K_S + S}\frac{O_2}{K_{O_2} + O_2}. \tag{2.1}$$

where μ_{max} is the maximum specific growth rate, K_S the affinity constant for substrate and K_{O2} the affinity constant for oxygen. Note that these *constants* are empirically determined and correspond to population averaged values (Ferenci, 1999a).

(vi) At the cell scale, the uptake rates differ from one cell to another as revealed by Natarajan and Srienc (2000). However, as stated in the Introduction, the overall uptake rate is algebraically linked to the population growth rate at steady state.

(vii) During the transition period, the population specific growth rate relaxes toward the equilibrium growth rate defined by Eq. (2.1). The shape of this adaptation in a biological-systems context is discussed in Morchain et al. (2013) and Morchain (2017).

2.2. *2-D population balance model*

Let $\xi \in \mathbb{R}^2$ be a set of internal properties that fully characterize a cell's state. For the sake of completeness, the cell growth is explored in a continuous and perfectly mixed bioreactor, characterized by its dilution rate D (1/h). The PBM for such a population reads

$$\frac{\partial}{\partial t}\mathcal{N}(t,\xi) + \nabla_\xi \cdot [\dot{\xi}\mathcal{N}(t,\xi)] + D\mathcal{N}(t,\xi) + \gamma(\xi)\mathcal{N}(t,\xi) = 2 \int \gamma(\xi')K(\xi,\xi')\mathcal{N}(t,\xi')\cdot d\xi' \tag{2.2}$$

where

$\xi = (l, v)^T$ is the vector of internal properties,

$\mathcal{N}$ is a number density function, and $\mathcal{N}(t, l, v)dldv$ is the number of cells with a rate of anabolism v and length l at time $t > 0$,
$\dot{\xi}$ is the vector of velocities in the space of internal variables, namely $\dot{l} = \partial l/\partial t$ and $\dot{v} = \partial v/\partial t$,
$\gamma(\xi)$ is the rate of cell division, and
$K(\xi, \xi')$ is a redistribution kernel that defines the probability that a cell in state ξ' gives birth to a cell in state ξ.

The factor 2 on the right-hand side of the equation indicates that one mother cell produces to two daughter cells. The boundary condition assumes a regularity condition (i.e. $\int_{\partial\Omega} \dot{\xi}_k \mathcal{N}(t, \xi) = 0 \quad \forall k \in \{1, \ldots, n\}$), and the initial condition $\mathcal{N}(0, l, v)$ belongs to $L^1(\mathbb{R}_+, [0, v_{max}])$.

In order to get the full set of equations for the dynamic simulation of a continuous bioreactor, the PBM is complemented with two mass balances for the carbon substrate, S, and the dissolved oxygen, O_2:

$$\frac{dS}{dt} = D(S_f - S) - \frac{\rho_c \pi d^2}{4} \iint q_S l \mathcal{N}(t, l, v) \cdot dldv \tag{2.3}$$

$$\frac{dO_2}{dt} = K_L a(O_2^\star - O_2) - DO_2 - \frac{\rho_c \pi d^2}{4} \iint q_{O_2} l \mathcal{N}(t, l, v) \cdot dldv \tag{2.4}$$

where ρ_c is the density of cells (assumed constant and equal to 1000 kg/m^3), q_S and q_{O_2} are the substrate and oxygen specific uptake rates, respectively, S_f is the substrate concentration in the feed (g/L), and $O_2^\star$ is assumed constant and given by Henry's law. The reader should note that all mass densities are given in kg/m^3, but are converted into g/L in the simulations. These mass balances are coupled to the PBM through the integral terms on the right-hand sides, which represent the contribution of the entire population. We may recall here that $\rho_c \pi d^2 l/4$ is a cell mass.

2.3. *Modelling the cell division*

Many breakage laws have been implemented in the literature (Hatzis et al., 1995; Fadda et al., 2012; Subramanian et al., 1970). Here, following Mantzatis (2006), we take

$$\gamma(l) = \left(\frac{l}{l_c}\right)^\kappa \tag{2.5}$$

where l_c is a constant characteristic length and κ, a shape parameter, is set to 5 as proposed by Mantzatis (2006). This smooth function allows cells to grow up to a length comparable to l_c, and cell division is almost guaranteed at $l = 2l_c$. However, it does not theoretically preclude the possibility that a cell never stops growing. The value of the parameter l_c is set to 10^{-5} m according to Nobs and Maerkl (2014).

2.4. *Modelling velocities in the internal phase space*

The length change is taken to be proportional to the rate of anabolism:

$$\dot{l} = \frac{\partial l}{\partial t} = a \min(v, \mu^\star). \tag{2.6}$$

This formulation ensures that a cell elongates at a rate proportional to the rate of anabolism under the condition that the medium is not depleted in carbon substrate and/or oxygen. The time scale associated with this elongation is the interdivision time. Since the elongation rate v is a distributed property, it results that the combination of (2.5) and (2.6) will produce the experimentally observed interdivision time distribution (Yasuda, 2011; Nobs and Maerkl, 2014).

The parameter a is a conversion constant that connects the rate of anabolism to the rate of elongation. This value is clearly strain dependent and, in the present work, it is adjusted to the total cell mass measured in the experiments simulated (see Table 1 for parameter values).

The relationships (1.3) and (1.4) reflect the well-established fact that the uptake rate is proportional to the specific growth rate at steady state. The latter is correlated to the residual substrate concentration. However there is much experimental evidence that the specific growth rate (and hence the elongation rate) is not correlated to the substrate concentration in the transient regime (see Perret, 1960; Abulesz and Lyberatos, 1989; Patarinska et al., 2000; Kätterer et al., 1986; Guillou et al., 2004 for the response to a step-up in the feed concentration or the dilution rate, and Adamberg et al. (2009) for the response to a gradual increase of the dilution rate). In fact, cells adapt their rate of anabolism in response to changes in environmental concentrations. The dynamics of such an adaptation has been investigated in previous works and the following expression was proposed and validated against experimental data (Morchain and Fonade, 2009; Morchain et al., 2017):

$$\dot{v} = \frac{\partial v}{\partial t} = \begin{cases} \left(\frac{1}{T} + v\right)(\mu^\star - v) & \text{if} \quad v \le \mu^\star \\ \frac{1}{T}(\mu^\star - v) & \text{if} \quad v \ge \mu^\star \end{cases} \tag{2.7}$$

where $\mu^\star$ is given by Eq. (2.1). The value of the parameter T was found to be around $1.25/\mu_{max}$.

2.5. *Modelling the redistribution kernels*

The redistribution kernel $K(\xi, \xi')$ accounts for the probability that a mother cell with internal variables ξ' gives birth to a daughter with internal variables ξ. Without precise empirical knowledge of the redistribution process of internal variables, we assume that the cell length and the rate of anabolism are independently redistributed at cell division. Thus, the redistribution kernel is a tensor product of two independent kernels, each one involving one internal variable. This leads to $K(\xi, \xi') = P(l, l')Q(v, v')$ with P being the length redistribution kernel, and Q the rate of anabolism redistribution kernel.

In general, $P(l, l')$ and $Q(v, v')$ satisfy the following properties:

$$\begin{aligned} &P(l, l') = P(l' - l, l'), \\ &\int_0^{l'} P(l, l') \cdot dl = 1, \\ &\int_0^{v_{max}} Q(v, v') \cdot dv = 1. \end{aligned} \tag{2.8}$$

The first states that a cell gives birth to two daughters cells, and the two others are normalization constraints. In this work, the redistribution kernel in length is

$$P(l, l') = \left(\frac{l}{l'}\right)^{m-1} \left(1 - \frac{l}{l'}\right)^{m-1} \frac{(2m-1)!}{(m-1)!^2} \tag{2.9}$$

with $m = 10$, so that P is a beta distribution centred around $l'/2$. We recall here that the cell division occurs around the

Table 1 – The parameter values used in the simulations.

Name	Value	Units	Description	Ref.
d	10^{-6}	m	Cell diameter	Assumed
l_c	10^{-5}	m	Critical length for the cell division rate	(Nobs and Maerkl, 2014)
v_{max}	1	h^{-1}	Maximal rate of anabolism	Assumed
κ	5	None	Stiffness in the cell division rate	(Mantzatis, 2006)
a	6.51×10^{-6}	m	Cell lengthening	Assumed
σ	10^{-2}	None	Variance in the redistribution kernel for v	Assumed
m	10	None	Parameter in the length redistribution kernel	Assumed
T	$\frac{1.25}{\mu_{max}}$	h	Characteristic time of adaptation	(Morchain, 2017)
t_M	50×10^{-3}	s	Micromixing time	(Morchain et al., 2017)
k_{cat}	6.15×10^{-6}	g_S permease^{-1} h^{-1}		Assumed
α_{max}	100	permease/m^2	Maximum permease surface density	Assumed
D	0.15	h^{-1}	Dilution rate	Assumed
k_{PTS}	0.01	g/L	PTS affinity constant	(Ferenci, 1996)
k_{Perm}	10^{-3}	g/L	Permease affinity constant	(Ferenci, 1996)
μ_{max}	0.46	h^{-1}	Maximum specific growth rate	(Sunya et al., 2012)
K_S	0.01	g/L	Macroscopic affinity constant for glucose	(Sunya et al., 2012)
K_{O_2}	10^{-4}	g/L	Macroscopic affinity constant for oxygen	Assumed
Y_{SX}	1/0.42 = 2.38	g_S/g_X	Substrate into biomass yield	(Sunya et al., 2012)
$K_L a$	300	h^{-1}	Global gas–liquid transfer rate	Identified (Sunya et al., 2012)
$O_2^\star$	8×10^{-3}	g/L	O_2 partial pressure in the gas phase	Henry's law

characteristic length l_c appearing in the definition of $\gamma(l)$. The kernel for the rate of anabolism is such that the daughter's rate is distributed around that of the mother cell according to a truncated Gaussian distribution:

$$Q(v, v') = \frac{\exp\left[-\frac{1}{2\sigma^2}(v' - v)^2\right] \mathbf{1}_{0 \le v \le 1}}{\int_0^{v_{max}} \exp\left[-\frac{1}{2\sigma^2}(v' - v)^2\right] dv}. \tag{2.10}$$

The variance is set arbitrarily to $\sigma = 10^{-2}$ in order to limit the randomizing effect of cell division on the rate of anabolism. With few experimental data regarding this parameter, it was assumed here that v is evenly distributed by the daughter cells, which therefore inherit a state rather similar to their mother's.

2.6. *Uptake rate models*

The formulation of an suitable uptake model expressed as a function of the cell properties and the available substrate is a key issue. Indeed, the uptake model actually defines the rate of mass transfer between the abiotic and the biotic phases; it consequently plays the role of a closure law for the set of Eqs. (2.2) and (2.3). In this paper, following Ferenci (1996), we consider here two mechanisms contributing to the glucose uptake at a cell's membrane:

(i) PTS are responsible for the substrate uptake at high S,
(ii) Permeases are instead characterized by a smaller affinity constant, which makes this system more efficient at low S.

These processes ease the cell's adaptation to the local environment and take into account the anticipatory effect that allows cells to ratchet up/down their backbone metabolism. When glucose is omnipresent, cells favour the sugar specific PTS system, whereas starvation triggers the non-selective option that consists in increasing the membrane permeability to allow the uptake of various carbon sources into the cell.

Accordingly, in this work, it is proposed that the uptake capacity ϕ_S of the cells takes the form

$$\phi_S = Y_{SX}\left[r_{PTS}\frac{S}{k_{PTS}+S} + \alpha(v,S)\frac{4}{\rho d}k_{cat}\frac{S}{k_{Perm}+S}\right] = \phi_{PTS} + \phi_{perm}. \tag{2.11}$$

The first term accounts for the PTS contribution to the overall substrate absorption. The second one models the permease transport system. Both correspond to active transport and are mediated by an enzymatic process with its own affinity constant. Therefore, k_{Perm} and k_{PTS} are defined at the cell scale. The ratio $4/(\rho_c d)$ corresponds to the cell surface-to-mass ratio, valid for rod-shaped cells. Thus α indicates the permease density (number of permeases per surface unit), bounded above by a maximum value α_{max}. k_{cat} is a rate constant for the substrate uptake through one permease (g_S permease^{-1} h^{-1}). The value of these parameters have been set in order that both contributions are comparable in the interval $S \in [k_{Perm}, k_{PTS}]$ (see Table 1).

In (2.11), the PTS uptake rate is defined by

$$r_{PTS} = \frac{\mu^\star + \min(v, \mu^\star)}{2} \tag{2.12}$$

This formulation is inspired by the work of Chassagnole et al. (2002) in which the uptake through PTS was correlated to both the external glucose concentration and the ratio Phosphoenolpyruvate (PEP)/Pyruvate(PYR). The transformation of PEP into PYR is the node connecting the glycolysis pathway to the TCA Cycle. The carbon flux that can enter this cycle is dependent on the availability of an electron acceptor (namely oxygen, if present). In case of oxygen depletion, the assimilation capacity through the PTS system is thus hindered by the accumulation of PEP whose conversion is slower because of insufficient energy. However, on short time scales, the pool of PYR may allow a transient boost in the carbon uptake through the PTS system in response to a glucose pulse. Rather than using a complex dynamical model for this, we propose the formulation (2.12) in which the absence of oxygen will limit uptake whilst allowing a transient over-assimilation if oxygen is present. The dependence on v ensures that the uptake rate through the PTS system, r_{PTS}, reaches an equilibrium value at steady state. At equilibrium, the population average specific growth rate $\tilde{v}$ equals the optimal growth rate $\mu^\star$. Thus one obtains that the equilibrium value of r_{PTS} equals $\mu^\star$, reflect-

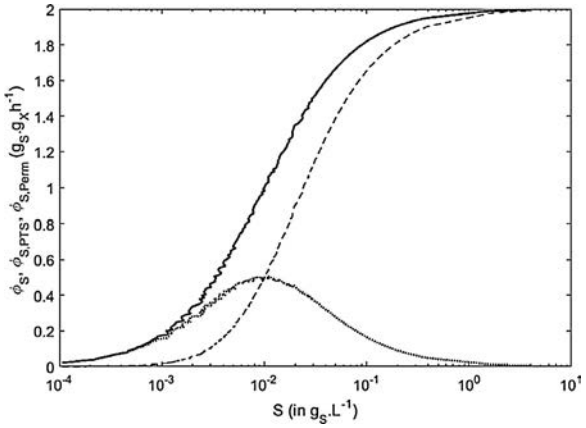

Fig. 1 – Total uptake q_S (solid) and respective contributions of the PTS (dashed) and permeases (dotted) as a function of residual substrate concentration S.

ing that the PTS system adjusts itself to allow for the optimal growth rate under the given environmental conditions.

In (2.11), the assumed permease density distribution is

$$\alpha(\upsilon, S) = \alpha_{\max} \exp\left(-\frac{\alpha_{\max}}{u}\upsilon\right) \tag{2.13}$$

where α_{max} is a constant parameter that reflects the cell's membrane permeability, and u obeys the dynamical equation

$$\frac{du}{dt} = -\frac{1}{\tau}(\tilde{q_S} - Y_{SX}\tilde{\upsilon}) \tag{2.14}$$

with a constant characteristic time τ that controls the time scale of change in the membrane permeability. The driving force of this adaptation is the difference between the overall substrate uptake rate and the overall population need. Here the notation $\tilde{\cdot}$ stands for the average over the whole population.

Fig. 1 shows the cells' more efficient glucose uptake mechanism as a function of the residual substrate concentration. This figure is found from a simulation of chemostat cultures at various dilution rates leading to different residual substrate concentrations. At low S, the majority of the total capacity ϕ_S is the contribution of the permeases, whereas the latter are inhibited by the PTS at high S, entailing a decrease in the ϕ_{perm} during the ϕ_{PTS} uptick. The rationale behind the above assumptions is that at the single-cell level, the available substrate that is likely to be absorbed is determined by phenomena operating at different scales: (a) meso/micromixing, (b) the effect of neighbouring cells, and (c) the cell's growth history (the so-called memory effect). The biological meaning of α is to represent a multiscale quantity. Thus, it is a function of the cells internal properties, but is heavily influenced by the hydrodynamics that affect the available amount of substrate at the cell membrane. It consequently blends mesoscopic and microscopic phenomena and operates upon a mechanical and physiological boundary. The permease density distribution is implemented such that at small D (entailing a small $\tilde{\upsilon}$), the substrate uptake is controlled by the permease (i.e. $\alpha(\tilde{\upsilon}, \tilde{S})$ is substantial), whereas at high D, $\alpha(\tilde{\upsilon}, \tilde{S})$ will be negligible in comparison to the PTS system that then yields the majority of the overall assimilation. These features fit the observations by reported by Ferenci (1996), Ferenci (1999b) and Kovàrovà-Kovar and Egli (1998).

Fig. 2 illustrates the contributions of PTS and permeases to the total uptake as a function of the rate of anabolism. Here, for demonstration purposes, it is assumed that the $\mathcal{N}(t, l, \upsilon)$ distribution is Gaussian and this distribution is normalized by its maximum value. The situation depicted is that of a population at steady state in a chemostat at $D = 0.15\,h^{-1}$. Thus the distribution is centred around $\tilde{\upsilon} = 0.15\,h^{-1}$. The normalized function $\alpha(S, \upsilon)/\alpha_{\max}$ decreases and consequently limits the role of permeases in the substrate uptake for those cells with a high rate of anabolism. On the contrary, for those cells with a lower rate of anabolism ($\upsilon = 0.15\,h^{-1}$), the permeases contribute to two thirds of the total uptake capacity. This feature of the model allows an overshoot in the uptake rate when starving cells are exposed to high substrate concentrations as has been observed experimentally (Lara et al., 2009; Neubauer et al., 1995).

2.7. *Interphase mass-transfer limitations*

A salient feature of the substrate uptake model proposed here is that we distinguish between the uptake capacity of the cell, ϕ_S, and the actual uptake, q_S, which can be limited by the transport of the substrate down to the cell scale. This limitation is due to the meso/micromixing that can hamper the uptake regardless the cells' capability to consume the substrate. This modelling approach, which has already been presented in previous work (Morchain et al., 2017), is based on the ratio of uptake and micromixing times. It states that the uptake rate is defined by

$$q_S = \phi_S\left[1 - \exp\left(-\frac{S}{S_c}\right)\right] \tag{2.15}$$

where the model for ϕ_S is ((2.11). The characteristic substrate concentration S_c is defined by (Morchain et al., 2017)

$$S_c = t_M Y_{SX}\tilde{\upsilon}X \tag{2.16}$$

with X the total biomass (calculated as an integral over the entire cell population), t_M the micromixing time (set to 50 ms in this study), and $\tilde{\upsilon}$ is the mean rate of anabolism of the population.

Following the same logic the actual oxygen uptake rate definition includes the possible limitation by the gas–liquid mass transfer:

$$q_{O_2} = \phi_{O_2}\left[1 - \exp\left(-\frac{K_L a O_2^\star}{X \quad \phi_{O_2}}\right)\right] \tag{2.17}$$

where $K_L a$ is a constant that takes into account the O_2 transfer from the gas phase to the liquid phase. Since O_2 is uptaken when glucose is absorbed by a cell and is not stored in the cytoplasm, ϕ_{O_2} is assumed equal to q_S, the eventual glucose uptake (a ratio of 1 g of oxygen per gram of glucose is assumed).

3. Numerical methods

The population balance (2.2) is solved with both a first-order finite-volume (FV) method and a Monte-Carlo (MC) algorithm. Throughout this section, the redistribution kernels $P(l, l')$ and $Q(\upsilon, \upsilon')$ are chosen beta and Gaussian, respectively. All codes are implemented in C++14.

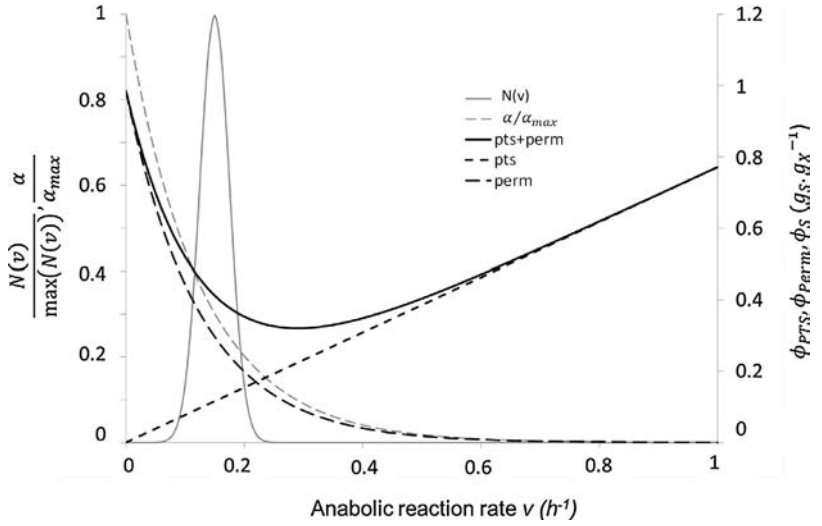

Fig. 2 – The function $\alpha(S, v)/\alpha_{max}$ (light grey dashed line) controls the induction of permeases for slow growing cells.

3.1. *The FV method*

The domain on which the PBM is solved is assumed to be a rectangle $[l_{min}, l_{max}] \times [0, v_{max}]$ and the PDF is computed on $(N+1) \times (M+1)$ nodes. In the following, $\mathcal{N}^n_{i,j}$ stands for the discrete approximation of $\mathcal{N}$ at time t^n and nodes $(l_i, v_j) \in [0, N+1] \times [0, M+1]$, and S^n the substrate concentration computed at time t^n. For the number density function, a classic local Lax–Friedrichs scheme was implemented:

$$\begin{aligned}\mathcal{N}^{n+1}_{i,j} = \; & \mathcal{N}^n_{i,j} - \frac{\Delta t}{\Delta l}\left(\mathcal{F}^n_{i+\frac{1}{2},j} - \mathcal{F}^n_{i-\frac{1}{2},j}\right) \\ & - \frac{\Delta t}{\Delta v}\left(\mathcal{G}^n_{i,j+\frac{1}{2}} - \mathcal{G}^n_{i,j-\frac{1}{2}}\right) - D\mathcal{N}^n_{i,j} - \gamma(l_i)\mathcal{N}^n_{i,j} \\ & + \Delta l \Delta v \sum_{i'>i}\sum_{j'\geq 0} \gamma(l_{i'})P(l_i, l_{i'})Q(v_j, v_{j'})\mathcal{N}^n_{i',j'}\end{aligned}$$

where $\mathcal{F}^n_{\cdot,\cdot}$ and $\mathcal{G}^n_{\cdot,\cdot}$ are the discrete fluxes associated to the respective advection contributions $\mathcal{F}(\dot{l}, \mathcal{N}) = \dot{l}\mathcal{N}(t, l, v)$ and $\mathcal{G}(\dot{v}, \mathcal{N}) = \dot{v}\mathcal{N}(t, l, v)$.

According to the Rusanov scheme, the fluxes explicitly read

$$\begin{aligned}\mathcal{F}^n_{i\pm\frac{1}{2},j} &= \frac{1}{2}\left(\mathcal{F}(\dot{l}^n_{i\pm1}, \mathcal{N}^n_{i\pm1,j}) + \mathcal{F}(\dot{l}^n_i, \mathcal{N}^n_{i,j})\right) + \frac{1}{2}\max(\dot{l}^n_{i\pm1}, \dot{l}^n_i)\left(\mathcal{N}^n_{i+1,j} - \mathcal{N}^n_{i,j}\right) \\ \mathcal{G}^n_{i,j\pm\frac{1}{2}} &= \frac{1}{2}\left(\mathcal{G}(\dot{v}^n_{j\pm1}, \mathcal{N}^n_{i,j\pm1}) + \mathcal{G}(\dot{v}^n_j, \mathcal{N}^n_{i,j})\right) + \frac{1}{2}\max(\dot{v}^n_{j\pm1}, \dot{v}^n_j)\left(\mathcal{N}^n_{i,j+1} - \mathcal{N}^n_{i,j}\right)\end{aligned}$$

The substrate concentration $S(t)$ is computed using a Riemann sum, with first-order integration at the domain boundary and second-order inside:

$$\begin{aligned}S^{n+1} = \; & S^n + \Delta t\Big(D(S_f - S^n) \\ & - \rho\pi\frac{d^2}{4}\Sigma\Sigma(l_i + l_{i+1}\mathbf{1}_{i<N})\left(\frac{v_j + \min(v_j, \mu^\star)}{2}\right) \\ & \left(\frac{v_{j+1} + \min(v_{j+1}, \mu^\star)}{2}\mathbf{1}_{j<M}\right)\frac{1}{(1+\mathbf{1}_{i<N})(1+\mathbf{1}_{j<M})} \\ & \left[(\mathcal{N}^n_{i,j} + \mathcal{N}^n_{i+1,j})\mathbf{1}_{i<N} + \mathcal{N}^n_{i,j+1}\mathbf{1}_{j<M} + \mathcal{N}^n_{i+1,j+1}\mathbf{1}_{\substack{i<N \\ j<M}}\right]\Big)\end{aligned}$$

When $O_2(t)$ reached small values, O_2^{n+1} was computed with the help of a semi-implicit scheme that removed the positivity challenge due to the term $K_L a(O_2^\star - O_2)$:

$$O_2^{n+1} = \frac{O_2^n + \Delta t K_L a O_2^\star - \Delta t\rho\sum_i\sum_j\pi\frac{d^2}{4}lq_{O_2}\mathcal{N}^n_{i,j}\cdot dldv}{1 + \Delta t(K_L a + D)}$$

3.2. *The MC method*

This Lagrangian tool was used in a test case for comparison with the results given by the FV code. Given an initial number of cells N_0 at $t = t_0$ whose values were Gaussian distributed, the procedure is the following:

(1) Set $t \to t + \Delta t$. An integer A is set equal to 0. A cell's residence time τ_i is given by the value of D and a random number v_i: $\tau_i = -\frac{\log(v_i)}{D}$.
(2) Random numbers u_i, $i \in \{0, \ldots, N_0 - 1\}$ are drawn from a uniform distribution. A is then set equal to $\sum_{0\leq i\leq N_0-1}\mathbf{1}_{u_i<1-\exp(-\Delta t\gamma_i)}$. If this sum is equal to 0, go back to 1).
(3) If $A > 0$, all magnitudes are computed using the explicit Euler method on the interval $[t_0, t]$. All ages a_i are also updated. Considering the set $B = \{i | u_i < 1 - \exp(-\Delta t\gamma_i)\}$, all cells with subscript in B will give birth to a daughter cell whose length, rate of anabolism and residence time are computed using respectively $P(l, l')$, $Q(v, v')$ and D. N_0 is also updated: $N_0 \to N_0 + |B|$.
(4) Considering the set $C = \{i | a_i > \tau_i\}$, all cells whose subscript lies in C are withdrawn from the reactor and $N_0 \to N_0 - |C|$.
(5) The last step is the update $t_0 \to t$ and the conservative resize with respect to the system's cardinal.

Fig. 3 illustrates the convergence of the two methods toward the same solution. The number of cells in the MC approach was limited to 20,000 which may explain the minor discrepancies.

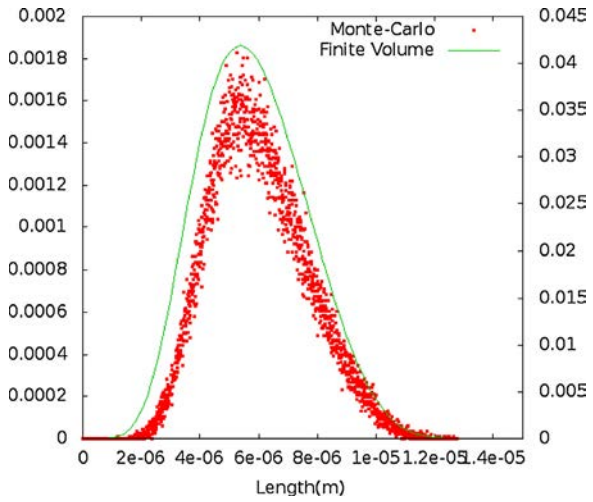

Fig. 3 – Comparison of the length distribution in an unlimited environment using different numerical simulation approaches.

4. Moments of the population balance

In this section, the moments of the population balance are introduced and used to demonstrate some properties of the PBM.

4.1. *Equivalence between growth in number and growth in mass*

Solving Eq. (2.2) is equivalent to solving the infinite set of equations on its moments. The moments of the $\mathcal{N}(t, l, v)$ distribution are defined as follows:

$$m_{p,q}(t) = \iint l^p v^q \mathcal{N}(t, l, v) \cdot dl dv. \tag{4.1}$$

Thus, the moment $m_{0,0}$ refers to the total number of cells, and the moment $m_{1,0}$ corresponds to the total mass, since the cell mass is proportional to the cell length. Let us establish the equation for these two moments. Starting from the general PBM (2.2), we obtain after some mathematical manipulation described in detail in Appendix A the following relationships:

$$\frac{d}{dt}\iint \mathcal{N}(t, l, v) \cdot dl dv = -D \iint \mathcal{N}(t, l, v) \cdot dl dv + \iint \gamma(l)\mathcal{N}(t, l, v) \cdot dl dv, \tag{4.2}$$

$$\frac{d}{dt}\iint l\, \mathcal{N}(t, l, v) \cdot dl dv = -D \iint l\, \mathcal{N}(t, l, v) \cdot dl dv + \iint \dot{l}\, \mathcal{N}(t, l, v) \cdot dl dv. \tag{4.3}$$

In other words, the notation $\langle \cdot \rangle$ standing for the double integral over the entire population, (4.2) and (4.3) read

$$\frac{dm_{0,0}}{dt} = -Dm_{00} + \langle \gamma \mathcal{N} \rangle = -Dm_{00} + \frac{\langle \gamma \mathcal{N} \rangle}{m_{0,0}} m_{0,0} \tag{4.4}$$

$$\frac{dm_{1,0}}{dt} = -Dm_{1,0} + \langle \dot{l} \mathcal{N} \rangle = -Dm_{1,0} + \frac{\langle \dot{l} \mathcal{N} \rangle}{m_{1,0}} m_{1,0} \tag{4.5}$$

These two equations degenerate into a single one on condition that

$$\frac{\langle \gamma \mathcal{N} \rangle}{m_{0,0}} = \frac{\langle \dot{l} \mathcal{N} \rangle}{m_{1,0}} \tag{4.6}$$

If the above condition holds, reasoning in terms of total cell mass or total cell number is equivalent.

At steady state ($\mathcal{N}(t, l, v) = \bar{\mathcal{N}}$), multiplying Eqs. (4.4) and (4.5) by the steady-state moments $\bar{m}_{1,0}$ and $\bar{m}_{0,0}$, respectively, and equating the two right-hand sides leads to

$$\bar{m}_{1,0}\left(-D\bar{m}_{0,0} + \langle \gamma \bar{\mathcal{N}} \rangle\right) = \bar{m}_{0,0}\left(-D\bar{m}_{1,0} + \langle \dot{l} \bar{\mathcal{N}} \rangle\right) \tag{4.7}$$

This equation can be rewritten in the same form as Eq. (4.6), so one condition for the growth in mass and in number to be equivalent is that the continuous culture is at steady state.

In a batch culture ($D = 0$), Eqs. (4.4) and (4.5) reduce to

$$\frac{1}{m_{00}}\frac{dm_{00}}{dt} = \frac{\langle \gamma \mathcal{N} \rangle}{m_{0,0}}, \tag{4.8}$$

$$\frac{1}{m_{10}}\frac{dm_{1,0}}{dt} = \frac{\langle \dot{l} \mathcal{N} \rangle}{m_{1,0}}. \tag{4.9}$$

It was well documented in Perthame (2007) and references therein that the number density function converges to a distribution whose geometry is shaped by the eigenvector associated to the population balance equation's largest eigenvalue (the so-called Malthus parameter). Then, for unlimited growth, the distribution becomes self-similar (Subramanian et al., 1970), meaning that

$$\frac{1}{m_{00}}\frac{dm_{00}}{dt} = 0.$$

The length distribution also remains self-similar, what yields

$$\frac{1}{m_{10}}\frac{dm_{10}}{dt} = 0.$$

Combining (4.8) and (4.9) then leads to the relationship

$$\frac{1}{m_{00}}\frac{dm_{00}}{dt} = \frac{1}{m_{10}}\frac{dm_{10}}{dt} \Rightarrow \frac{\langle \gamma \mathcal{N} \rangle}{m_{0,0}} = \frac{\langle \dot{l} \mathcal{N} \rangle}{m_{1,0}}. \tag{4.10}$$

Therefore, we have demonstrated that the population specific growth rate in number equals the population specific growth rate in mass if the culture is at steady state or if the population is growing exponentially.

4.2. *On the relationship between the 2-D and population-averaged model*

The usual unstructured model (or population-averaged model) takes the following form:

$$\begin{aligned} \frac{dX}{dt} &= (\mu - D)\, X, \\ \frac{dS}{dt} &= D(S_f - S) - Y_{SX}\mu X, \\ \mu &= \mu_{\max}\frac{S}{k_{PTS} + S}. \end{aligned} \tag{4.11}$$

Dividing Eq. (4.3) by the volume of liquid produces an equation for the cell concentration X (in g_X/L) very similar to the corresponding equation of the standard unstructured model

(4.11). However, these two equations are not equivalent and the unstructured model equation results from an approximation used to simplify the last term of Eq. (4.3):

$$\iint \dot{l}\mathcal{N}(t,l,v)\cdot dl dv = \iint \left(\frac{\dot{l}}{l}\right) l\mathcal{N}(t,l,v)\cdot dl dv$$
$$\approx \left(\frac{\dot{l}}{l}\right) \iint l\mathcal{N}(t,l,v)\cdot dl dv = \mu X. \quad (4.12)$$

In other words, the integral of the cell growth rate in mass over the population is roughly expressed as the product of the total mass multiplied by an average specific growth rate. This is only a rough approximation which, however, is justified if $\dot{l}/l$ is constant, meaning that the growth is exponential.

This observation clarifies the definition of μ as it appears in the standard unstructured model. For that model to be exact, μ should always be equal to $\langle \dot{l}\mathcal{N}\rangle / m_{1,0}$ (see Eq. (4.5)), whilst there is no information on the distribution in the unstructured modelling approach. It is therefore of no surprise that the unstructured model is not suitable to predict the transient behaviour of cell populations. One can further observe that cell division modifies the distribution $\mathcal{N}$, but leaves the total mass unchanged. Because μ in Eq. (4.11) is defined on a mass basis, it is not possible to investigate the consequences of any process that would impact the cell number and the cell mass on separate time scales. Clearly, the mass transfer from the liquid to the cell (uptake) is one such phenomena since uptake obviously precedes cell division. As a matter of fact, it is a paramount interest to recall that the relationship between growth and uptake rates is made on a mass basis, whereas the exact definition of specific growth rate is made on a number basis, i.e.,$\bar{\mu} = \ln 2/t_d$

The discussion above shows that (4.11) comes down to approximating an integral over the population by the product of the averaged quantities, the latter being only first-order accurate. This approximation is good for $t \to \infty$, but it can be highly inaccurate if the system is disturbed from the outside, for instance if a pulse of substrate is injected into the reactor. The first-order approximation in this case is misleading for it states that the specific growth rate immediately ratchets up from an equilibrium value to an algebraic $\mu(S(t))$. Because no distinction is made between cell mass and cell number, any gain in mass (uptake) is translated immediately into a higher specific growth rate which turns into a higher cell concentration which is simply inaccurate based on experimental observations.

5. Results and discussion

In this part, we first perform a series of experiments to test our model behaviour in response to a pulse under fully aerobic conditions. Then we assess our model against experimental data obtained by Sunya et al. (2012). A population of *E. coli* cells is set to equilibrium in a chemostat. Pulsed addition of substrate with various intensities (0.08, 0.4 and 1 g/L) are imposed on the cell population. The macroscopic properties of cell growth were given by the authors ($\mu_{max} = 0.46\,h^{-1}$, apparent substrate affinity $K_S = 0.01$ g/L, substrate to biomass yield at steady state $Y_{XS} = 0.42\,g_X/g_S$). The oxygen concentration in the liquid phase was measured with a fast responding probe, the oxygen and CO_2 concentrations in the outlet gas flow were obtained from a gas analyser. Glucose, acetate and formate were also analyzed at high temporal resolution using a mass spectrometer.

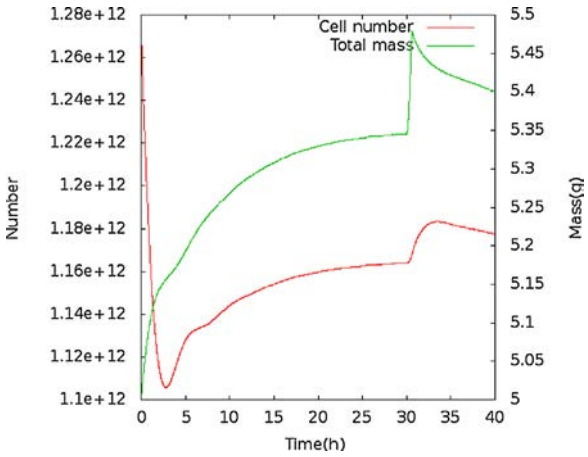

Fig. 4 – Evolution of the total mass and total number of cell during the continuous culture.

The parameter values used in simulations are reported in Table 1.

5.1. *Pulse addition without oxygen limitation*

In this part, oxygen is set constant, equal to its saturation value so that it has no impact on the results. A continuous culture at $D = 0.15\,h^{-1}$ is simulated and a pulse of substrate of 1 g/L is imposed at $t = 30$ h. We present the evolution of the integral properties of the cell population (mass, number) as well as the distributions in length and rate of anabolism before the establishment of a steady-state.

Interestingly, one can observe in Fig. 4 that the total mass and total number evolve separately and eventually tend to become proportional when the culture approaches steady state. From that point onward, examining the population growth on a number or on a mass basis becomes equivalent since the average cell mass is now time independent. Fig. 5 shows that the distributions in length and rate of anabolism become self-similar at the end of the preliminary phase that precedes the pulse addition.

The pulse addition of substrate results in a instantaneous increase in the cell mass because all cells can now elongate at their potential rate v instead of being limited by the environment (see Eq. (2.6)). However the evolution in terms of total cell number is not so sudden since cells have to elongate before they can divide into two daughter cells. Fig. 6 presents a closer view of this decoupling between growth in mass and growth in number.

These numerical results were theoretically predicted in Section 4. Note also that the slight differences in terms of number and mass between Figs. 4 and 6 are due to a change in the parameter lc which indirectly controls the average cell size and hence the total cell mass at steady-state.

5.2. *Pulse addition with oxygen limitation: comparison to experimental data*

In this part, glucose, oxygen, cell mass and cell number are calculated. A constant $K_L a = 300\,h^{-1}$ was deduced from the experimental data at steady state prior to the glucose pulse. Integrating over the entire population leads to the total uptake rates for glucose and oxygen as well as the specific growth

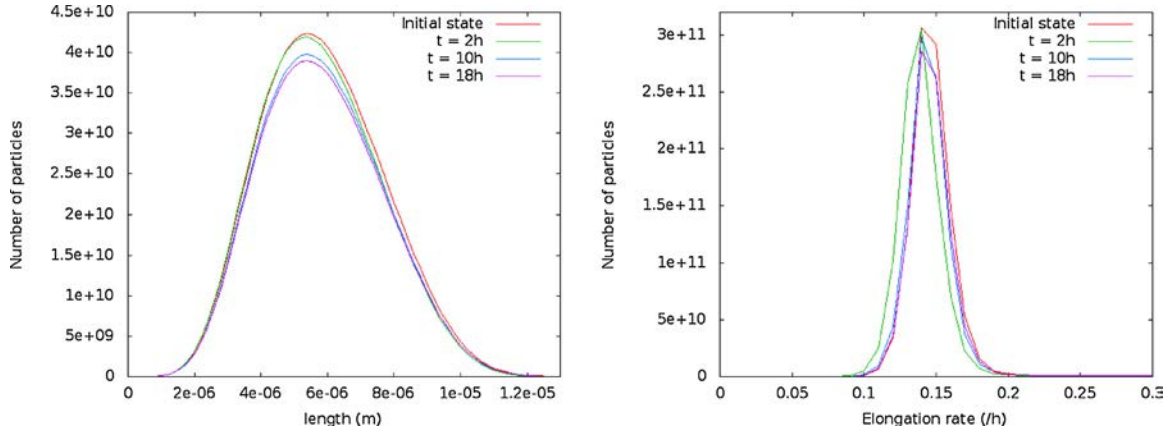

Fig. 5 – Distribution in length (left) and anabolism rate (right) toward steady-state. A population is cultivated in a chemostat ($D = 0.15$). For the sake of simplicity, the distribution were inferred before the simulation so that the code was only run for three times the residence time $1/D \approx 6.6$ h. Red: initial pdf; green: at $t = 2$ h; blue: at $t = 10$ h; purple: at $t = 18$ h. (For interpretation of the references to colour in this figure legend, the reader is referred to the web version of the article.)

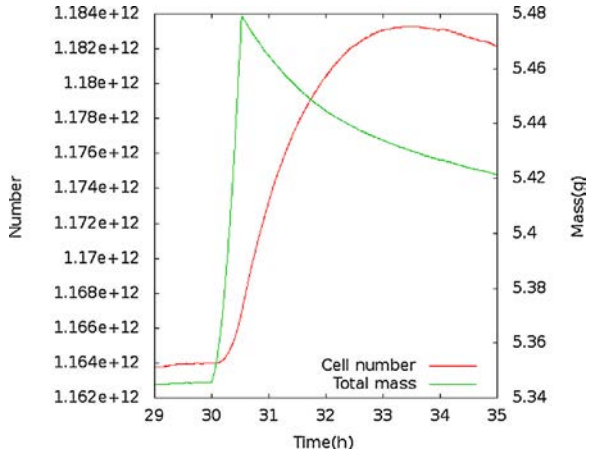

Fig. 6 – Evolution of the total mass and total number in response to a glucose pulse in a continuous culture.

rate in number and the rate of mass change due to cell growth (elongation).

Fig. 7 presents the evolution of the key variables of the dynamic response to a glucose pulse for the 0.4 g/L experiment. Just before the pulse, the PTS system contributes to approximately one third of the total glucose uptake (0.16 out of 0.37). Immediately after the pulse ($t < 0.1$ min), the total uptake rate jumps because of the PTS contribution. At that moment, oxygen is still present and this allows r_{PTS} to step-up and to overtake the contribution of permeases to the total transport. Because the glucose uptake rate has increased but the cell had hardly no time to change its rate of anabolism, the total glucose uptake rate now exceeds the glucose consumption due to anabolism. The permeases start shutting down, because of that excess carbon flux, according to Eq. (2.14). Oxygen depletion takes place at $t = 0.1$ min. As explained in the model presentation, the lack of oxygen slows down the catabolic activity and r_{PTS} falls down. Nevertheless, the still active permease system compensate the diminution of r_{PTS} so that eventually the total uptake rate remains stable. The plateau following the initial overshoot is clearly visible in the experimental data but remained unexplained until now.

From 1 to 10 min, the glucose concentration linearly decreases which progressively reduces the demand for oxygen. Thus the dissolved oxygen concentration slightly increases, resulting in an increased catabolic activity. Hence r_{PTS} goes up and permeases keep closing for the same reason as before (uptake exceeds the cell needs for anabolism). At substrate exhaustion, the rapid decrease of the sugar concentration creates a situation where q_S becomes smaller than $Y_{SX}.\upsilon$, so the cell receive a signal that the substrate flux into the cell becomes insufficient with respect to the cell needs (note that the concentration does not have to be extremely low for that message to be recorded by the cell (see Ferenci, 1996). This insufficient carbon flux signal triggers the increase in the permease activity. It is very interesting to observe that the dynamic model predicts that, as the sugar gets exhausted, the permease activity increases which explains how cells can anticipate the glucose exhaustion and manifest an apparent "anticipation capacity". This important characteristic of our model is clearly a benefit from a flux formulation in Eq. (2.14).

Fig. 8 shows the prediction of our numerical model compared to the experimental data for the three pulse intensities. In the simulation, the glucose uptake rate is slightly underestimated. The agreement is rather satisfying and we were particularly interested in understanding the origin of such similar uptake rates, irrespective of the pulse intensity. We came to the conclusion that the glucose uptake rate was in fact limited by the oxygen mass transfer during the experiments. Indeed, the maximum oxygen transfer rate is given by $K_L a O_2^*$. Considering the $K_L a$ value identified from the steady state concentrations, we conclude that the oxygen uptake rate is limited to 2.4 $g_{O_2}\,L^{-1}\,h^{-1}$ which closely matches the observed glucose consumption rate in all experiments (0.4 g in 10 min or 1 g in 25 min). This observation supports the assumption made in the model that 1 g of oxygen is consumed per gram of substrate uptaken.

In the simulations, the glucose uptake is limited by the low concentration of oxygen (see the role of O_2 in r_{PTS}). Therefore the whole dynamics is controlled by this residual concentration of oxygen whose value is highly dependent on the constant K_{O2}. Fig. 9 shows the evolution of the dissolved oxygen concentration as predicted by the model. It is put to the reader's attention that O_2 approaching zero hampers the glucose uptake. This underestimation of the glucose uptake rate is therefore related to the low oxygen residual concentration. A lower K_{O2} would cause the oxygen concentration to be much closer to zero and this would also adversely reduce the r_{PTS}. It appears that, the Monod kinetics states that the reaction stops if oxygen is zero whereas in fact the reaction

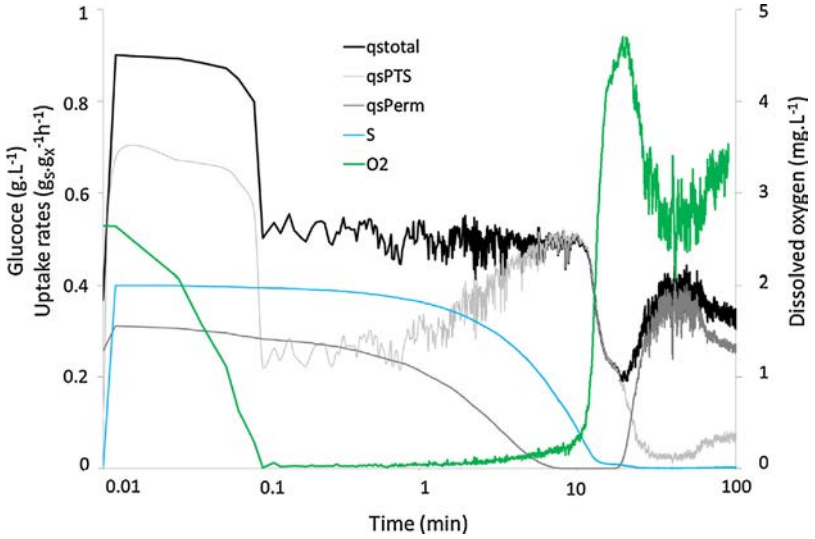

Fig. 7 – Dynamics of substrate uptake during the response to a pulse addition of 0.4 g/L of glucose in a chemostat at $D = 0.16h^{-1}$. A log scale is used for the abscissae to emphasize the first instants after the pulse. S and O_2 are represented in blue and green respectively, uptake rates are in light grey (PTS), dark grey (Permeases) and black (total).

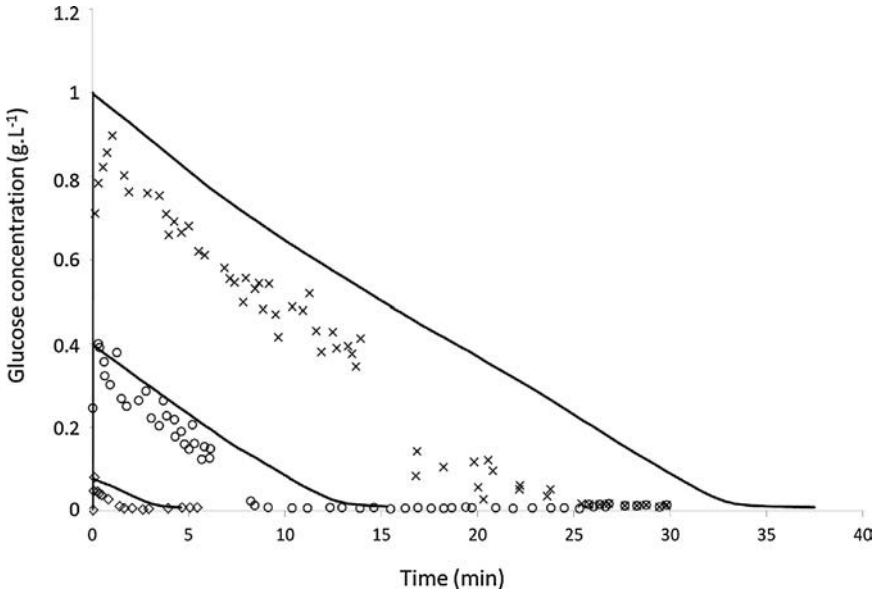

Fig. 8 – Response to a pulse of substrate of various intensities in a chemostat. Comparison of the model prediction to the experimental data of Sunya et al. (2012).

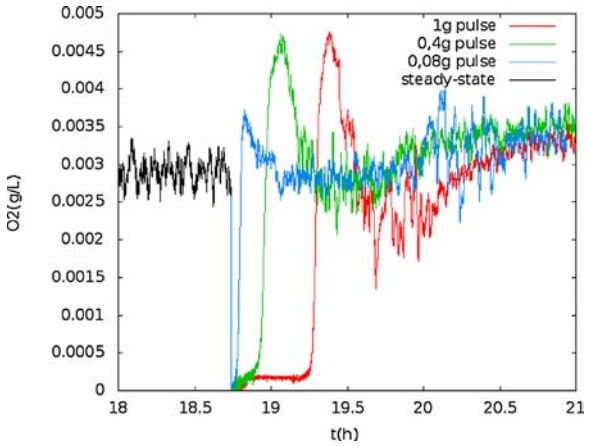

Fig. 9 – Simulated oxygen concentrations in the liquid phase as a function of time, shortly before and after the pulses.

rate would become limited by the gas-liquid mass transfer rate. This entails a caution related to the use of Monod laws to describe local phenomena in biology in general. The use of concentration in the kinetic law makes them unadapted to the situation where interphase mass transfer is the limiting phenomena. Actually, it would be preferable to avoid completely the use of Monod kinetics and to include a limitation of r_{PTS} by the maximum oxygen transfer rate without any reference to the residual concentration of oxygen. Furthermore, the use of concentration based kinetic rates creates some numerical noise that could not completely avoided despite the semi-implicit strategy for the resolution. The behaviour after glucose exhaustion is not representative of the experiments because the oxygen uptake associated to the reconsumption of acetate is not included in our model.

Fig. 10 gives an insight at which transport phenomenon drives the glucose uptake in function of the substrate flux entering the cells. At steady-state, $S \approx 5 \times 10^{-3}$ g/L, i.e. 5 times the permease affinity constant k_{perm} but only one half of k_{PTS}.

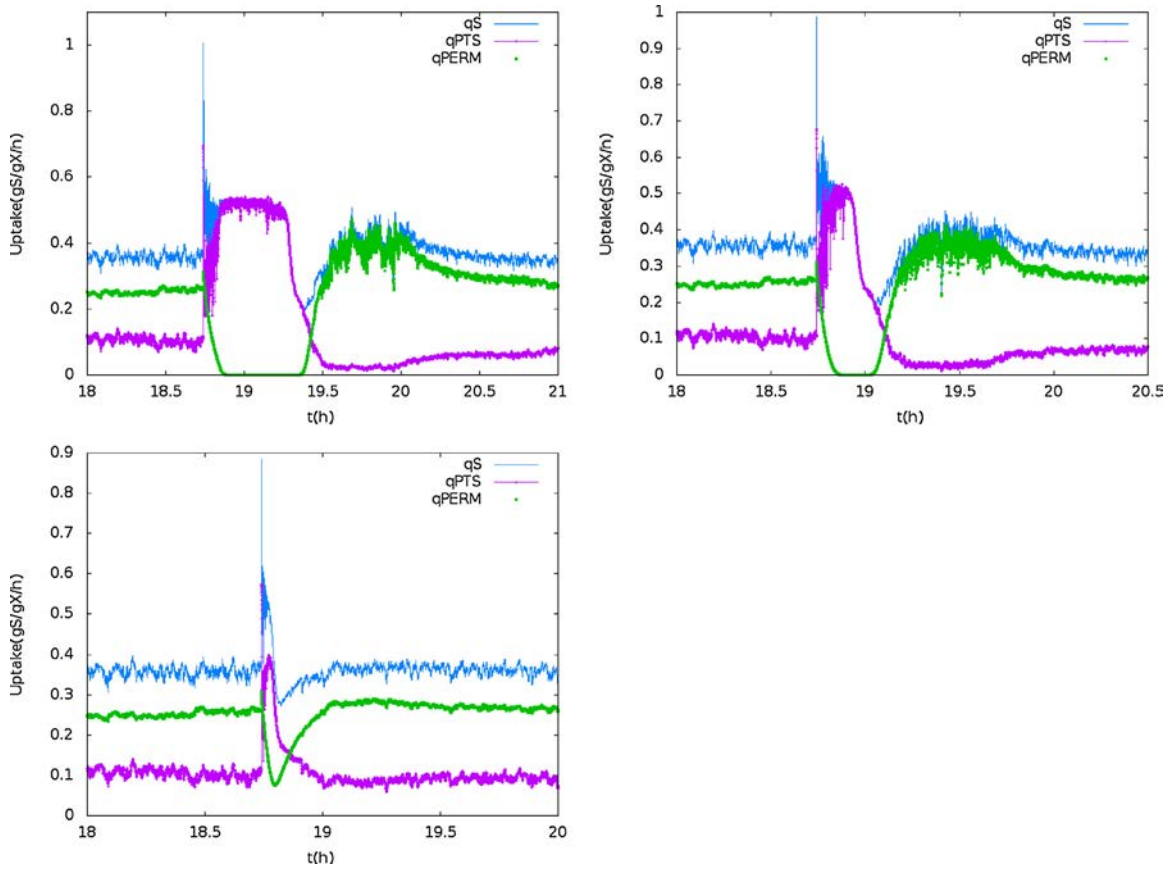

Fig. 10 – Total substrate uptake rate, PTS and Permeases contributions, shortly before and after the pulse. Top right: 1 g/L, top left: 0.4 g/L, bottom left: 0.08 g/L.

In this case, the permease contribution to the total q_S is 2–3 times over its PTS counterpart. The permease system in that case is already almost saturated. At the beginning of the pulse, the PTS are immediately requested and their full-on functioning ratchets up the q_S while the permeases' contribution does increase a little. In all cases, the instantaneous total uptake rate is multiplied by a factor 3 as reported in the experiments. Shortly after, the permeases' shutting leads to a plateau situation characterized by a PTS-only work. When $S \to 0$, the PTS becomes less and less effective and the permeases relay the PTS until steady-state is reached once again.

Up to now, it was shown that the glucose uptake was correctly predicted, it was explained why it was slightly underestimated and it was also shown that the gain in the total cell mass following a pulse addition of a subsequent amount of carbon is in contrast very limited (see Fig. 6). So there is an apparent contradiction between the quantitative uptake of substrate and the small increase in the total cell mass. This is not surprising in our model since there is no carbon balance over the cell. Such a balance could be implemented through a minimal metabolic modelling and although it is possible (see Pigou and Morchain, 2015), it was not the central objective in this paper. Nevertheless, the question of the fate of the uptaken carbon remains and we will see now how the experimental data provide a way to confirm our model prediction. For this purpose, a carbon mass balance was established from the experimental measurements of the carbon dioxide in the gas outflow and the concentrations of by-products excreted during the pulse. Fig. 11 presents the difference between the concentration in the gas phase during the pulse and the concentration measured at steady state. Since the duration of the glucose exhaustion is relatively small compared to the residence time, it can be assumed that the totality of the carbon transformed into CO_2 finally exits the reactor in the gas phase. We performed the integration of these curves and multiplied by the gas flow rate to quantify the amount of CO_2 produced during the pulse. Acetate and formate are also produced during the glucose excess period. However acetate is reconsumed and therefore also contribute to CO_2 production. This was taken into account in the mass balance. The results presented in Fig. 12 show that 65% of the total carbon uptaken is transformed into CO_2, acetate and formate during the 1 g/L pulse experiment. This fraction goes up to 93% for the 0.08 g/L pulse. The simultaneous consumption of oxygen during the period of high glucose uptake confirms the fact that the first response of the biological system is to transform the glucose uptaken in excess into CO_2. We can conclude that there is actually a significant uptake of carbon but a simultaneous release of CO_2 in the liquid phase. The carbon uptaken is not mainly metabolized to form new cells. Note that our model quantifies this excess through the difference $q_S - Y_{SX}\tilde{v}$.

In the 1 g/L pulse experiment, it can be calculated from the growth yield on glucose that the amount of carbon available for growth would correspond to a maximum of 0.11 g of new cells (assuming that Y_{SX} remains constant during the pulse). This value is obtained from the carbon mass balance excluding any storage, so it constitutes an upper limit. In our simulation, the boost in the uptake rate of substrate is not directly interpreted in terms of increase growth rate but we proposed that the dynamics of the population would be dictated by its rate of anabolism prior to the pulse. This hypothesis actually leads to a net production of biomass equal to 0.07 g after 25 min (glucose exhaustion). This results is therefore consistent with the carbon mass balance and confirms the fact that the substrate

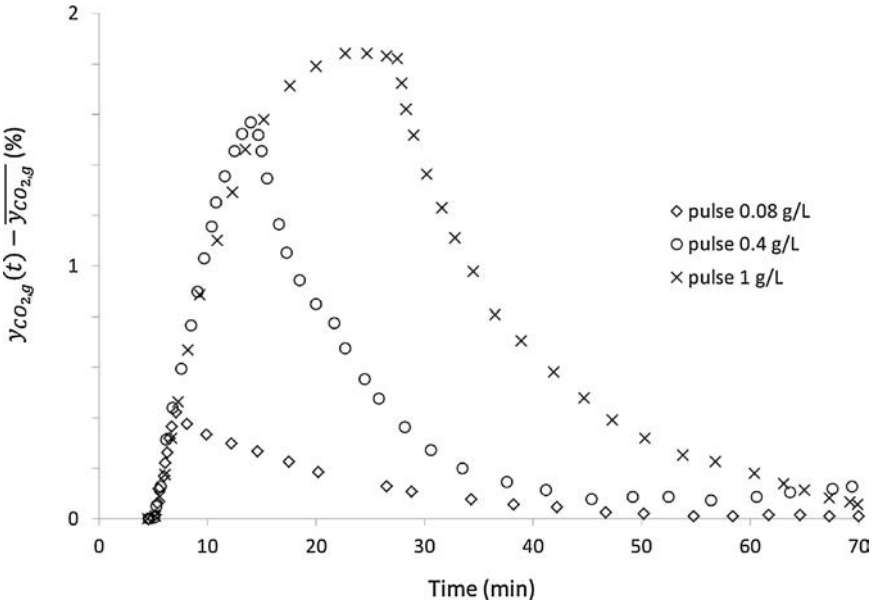

Fig. 11 – Relative change in the concentration of CO_2 in the gas phase during the pulse experiments. Data from Sunya et al. (2012).

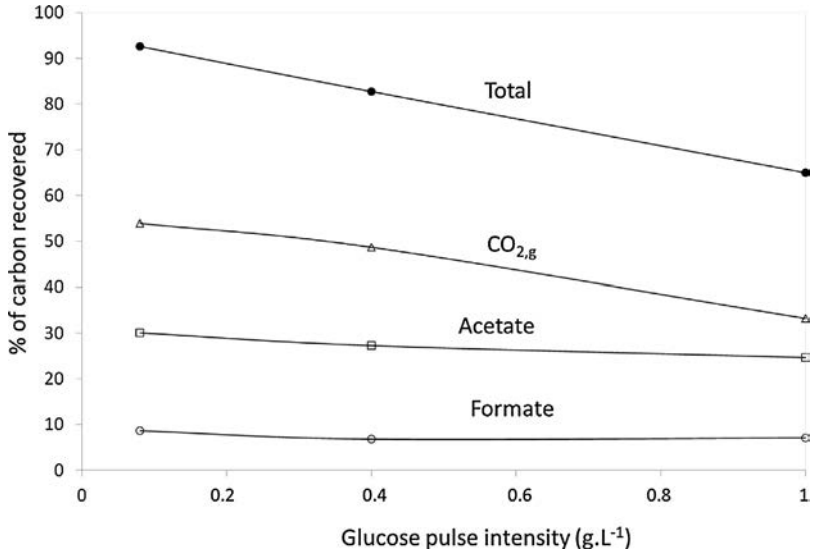

Fig. 12 – Carbon mass balance. Data from Sunya et al. (2012).

uptake rate was significant whilst the population gain in mass was in practice undetectable.

5.3. *The instantaneous uptake rate can exceed its maximum value observed in batch*

In order to model the permease contribution to the total q_S, a value for k_{cat} is inferred and entails an equilibrium value for α. Indeed, αk_{cat} is a constant factor that emerges from the steady-state equation:

$$\left(D\frac{\bar{S}}{\bar{S}+k_{PTS}}+\alpha k_{cat}\frac{4}{\rho d}\frac{\bar{S}}{\bar{S}+k_{Perm}}\right)\left(1-\exp\left(-\frac{\bar{S}}{S_c}\right)\right)=D$$

where $\bar{S}$ stands for the residual substrate concentration at steady-state. Therefore (D being given and assumed constant), the surge in q_{perm} in the wake of a glucose pulse is totally determined by k_{cat}: the higher it is, the lower α is at steady-state, the less is the permease overactivity following the disruption.

It is highlighted in Joseph (2005) that "genetic interventions usually lead to very large changes in enzyme activity". In other terms, the cells' membrane permeability can be altered in order that the total q_S overtakes the maximum value encountered in batch culture (here, $\upsilon_{max}/Y_{SX} \approx 1.095$).

The model's equivalent would be a decrease in k_{cat} that would lead to a higher value for α before the disruption. Consequently, in the seconds following a glucose pulse, the q_{perm} contribution to q_S would be high enough to allow q_S exceeding the maximum value in batch conditions.

This is indeed predicted by the model. Fig. 13 is testament to the response of a population cultivated at low (0.05) D (meaning that the permease transport accounts for the majority of the total uptake) to a step in S. k_{cat} was divided by 2 so that the permease are significantly open before the glucose step. The glucose uptake rate q_S ratchets up in the wake of the injection and momentarily surpasses υ_{max}/Y_{SX}.

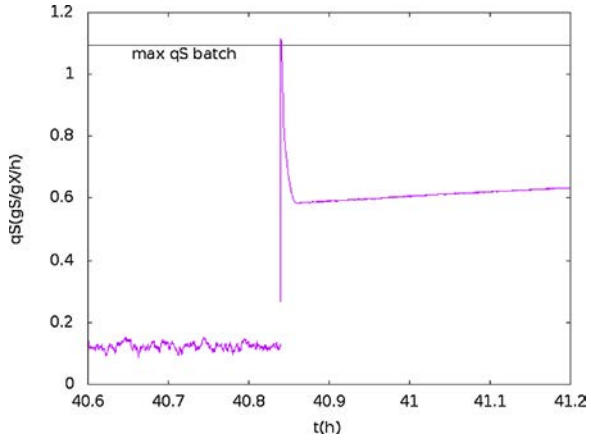

Fig. 13 – Instantaneous total substrate uptake rate following a 1 g/L pulse at $D = 0.05\ h^{-1}$.

6. Conclusion

This article highlights the relevance of a 2-D PBM formulated in terms of length (equivalent to mass for the rod-shaped cells) and rate of anabolism to investigate the population dynamics under transient conditions. The moments of the PBM were used to demonstrate that growth in mass and growth in number are only equivalent at steady-state in a continuous bioreactor and during the unlimited growth phase in a batch culture. In general, growth in mass is a matter of cell elongation (controlled by the rate of anabolic reactions) whereas growth in number is a matter of cell division (controlled by the cell division kernel). The proposed model allows for the description of transient behaviours of a cell population when growth in mass and growth in number are no longer equivalent. As an illustration, it is shown that the pulse addition of the carbon source in a substrate limited culture first causes an increase in the cell mass followed by an increase in the cell number. The second originality of this work is the formulation of an uptake law as the sum of two contributions standing for as many transport systems (PTS and permeases). Taking into account multiple transport systems is certainly necessary when modelling bacteria populations. In the proposed model, the contribution of each system to the total uptake evolves because of the difference between the actual substrate uptake and the cell needs for growth (deduced from the rate of anabolism). The dynamics of each system obey different time scales. This model compares favourably with experimental results. It is also consistent with experimental observation such as the apparent capacity of cells to anticipate the substrate exhaustion (Ferenci, 1996) or the fact that the instantaneous substrate uptake rate may exceed the maximum uptake rate observed in batch culture (Lara et al., 2009). As it is, the proposed model already appears as a valuable tool to understand and analyze one experimental data set existing in the literature. It could be observed that the dilution rate and pulse intensity are not sufficient to fully characterize the experiments. However, it is clear to the authors that some parts of the model need further improvements. A detailed sensitivity analysis has still to be conducted. It is also reasonable to include minimal energy and mass balances at the cell level. The ongoing works now concern the assessment of this model against various experimental data regarding substrate limited continuous culture at different dilution rate, different S/X ratio, inlet feed concentration and global mass transfer coefficients.

This model is now set to be implemented in a computational fluid dynamics (CFD) code to couple the biological behaviour to both micro and macro mixing. It will then be used as a tool to numerical simulations on a $\sim 10^5$ L-reactor routinely put in place in many industrial processes.

Acknowledgment

The authors gratefully acknowledge the financial support provided by the University of Toulouse via the IDEX program "Chaire d'attractivité", funded by the ANR.

Appendix A. Integral expression of the 2-D PBE

We provide below some details about the mathematical calculation of the integral expression obtained from the PBE (2.2). The passage from Eq. (2.2) to Eq. (4.3) is detailed first.

Regarding the cell number, an integration of (2.2) yields:

$$\frac{d}{dt}\iint \mathcal{N}(t,l,v)\cdot\cdot\,dl dv + D\iint \mathcal{N}(t,l,v)\cdot\cdot\,dl dv + \iint \gamma(l)\mathcal{N}(t,l,v)\cdot\cdot\,dl dv = 2\int\int\int\int_{l'>l} \gamma(l')P(l,l')Q(v,v')\mathcal{N}(t,l',v')\cdot dl'dv'\cdot dl dv \tag{A.1}$$

Indeed, the regularity boundary condition imposed on v leads to

$$\iint \frac{\partial}{\partial v}[\dot{v}\mathcal{N}(t,l,v)]\cdot dl dv = \int [\dot{v}\mathcal{N}(t,l,v)]_0^1 dl = 0$$

and its counterpart

$$\iint \frac{\partial}{\partial l}[\dot{l}\mathcal{N}(t,l,v)]\cdot dl dv$$

vanishes the same way.

Using the Fubini theorem to transform the right-hand side of (A.1) yields:

$$2\int\int\int\int_l^\infty \gamma(l')P(l,l')Q(v,v')\mathcal{N}(t,l',v')dl'dv'\cdot dl dv = 2\iint \gamma(l')\mathcal{N}(t,l',v')\{\int_0^{l'} P(l,l')dl\int Q(v,v')dv\}dl'dv'$$

Recalling the properties (2.8), the right-hand side takes the shape of:

$$2\int\int\int\int_l^\infty \gamma(l')P(l,l')Q(v,v')\mathcal{N}(t,l',v')dl'dv'\cdot dl dv = 2\iint \gamma(l')\mathcal{N}(t,l',v')dl'dv'$$

One can then rewrite (A.1):

$$\frac{d}{dt}\iint \mathcal{N}(t,l,v)\cdot dl dv = -D\iint \mathcal{N}(t,l,v)\cdot dl dv + \iint \gamma(l)\mathcal{N}(t,l,v)\cdot dl dv \tag{A.2}$$

Since it was assumed that a cell's mass is proportional to their length, an integration of the first moment on l of (2.2) gives the balance on the biomass. It reads:

$$\frac{d}{dt}\iint l\mathcal{N}(t,l,v)\cdot dldv - \iint \dot{l}\mathcal{N}(t,l,v)\cdot dldv + D\iint ln(t,l,v)\cdot dldv + \iint l\gamma(l)\mathcal{N}(t,l,v)\cdot dldv = 2\int\int\int\int_{l'>l}\gamma(l')lP(l,l')Q(v,v')\mathcal{N}(t,l',v')dl'dv'\cdot dldv \tag{A.3}$$

Indeed, an integration of the advection terms gives:

$$\iint l\frac{\partial}{\partial l}[\dot{l}\mathcal{N}(t,l,v)]\cdot dldv = -\iint \dot{l}\mathcal{N}(t,l,v)\cdot dldv$$
$$+\int [l\dot{l}\mathcal{N}(t,l,v)]_0^\infty dv = -\iint \dot{l}\mathcal{N}(t,l,v)\cdot dldv$$

having integrated by parts and used the regular boundary conditions, and

$$\iint l\frac{\partial}{\partial v}[\dot{v}\mathcal{N}(t,l,v)]\cdot dldv = \int l[\dot{v}\mathcal{N}(t,l,v)]_{v=0}^{v=1}dl = 0$$

Regarding the right-hand side of (A.3), another use of the Fubini theorem gives:

$$2\int\int\int\int_{l'>l}\gamma(l')lP(l,l')Q(v,v')\mathcal{N}(t,l',v')dl'dv'\cdot dldv =$$
$$2\iint\gamma(l')\mathcal{N}(t,l',v')\left\{\int_0^{l'}lP(l,l')dl\int Q(v,v')dv\right\}dl'dv'$$

To compute the integral over l, one uses the change of variables $l \to l' - l$:

$$\int_0^{l'}lP(l,l')dl = \int_0^{l'}(l'-l)P(l'-l,l')dl$$
$$= l'\int_0^{l'}P(l,l')dl - l\int_0^{l'}P(l,l')dl$$

using the hypothesis $P(l,l') = P(l'-l,l')$.

At the end of the day,

$$\int_0^{l'}lP(l,l') = \frac{1}{2}l'$$

and:

$$2\int\int\int\int_{l'>l}\gamma(l')lP(l,l')Q(v,v')\mathcal{N}(t,l',v')dl'dv'\cdot dldv$$
$$= \iint\gamma(l')\mathcal{N}(t,l',v')dl'dv'$$

References

Abulesz, E.M., Lyberatos, G., 1989. Periodic operation of a continuous culture of Baker's yeast. Biotechnol. Bioeng. 34 (September (6)), 741–749.

Adamberg, K., Lahtvee, P.-J., Valgepea, K., Abner, K., Vilu, R., 2009. Quasi steady state growth of *Lactococcus lactis* in glucose-limited acceleration stat (A-stat) cultures. Antonie van Leeuwenhoek 95 (3), 219–226.

Bell, G.I., Anderson, E.C., 1967. Cell growth and division I. A mathematical model with applications to cell volume distributions in mammalian suspension cultures. Biophys. J. 7, 329–351.

Chassagnole, C., Noisommit-Rizzi, N., Schmid, J.W., Mauch, K., Reuss, M., 2002. Dynamic modeling of the central carbon metabolism of *Escherichia coli*. Biotechnol. Bioeng. 79 (12), 53–73.

Eakman, J.M., Fredrickson, A.G., Tsuchiya, H.M., 1966. Statistics and dynamics of microbial cell populations. Chem. Eng. Prog. Symp. Ser. 69, 37–49.

Fadda, S., Cincotti, A., Cao, G., 2012. A novel population balance model to investigate the kinetics of in vitro cell proliferation: Part I. Model development. Biotechnol. Bioeng. 109 (3), 772–781.

Ferenci, T., 1996 July. Adaptation to life at micromolar nutrient levels: the regulation of *Escherichia coli* glucose transport by endoinduction and cAMP. FEMS. Microbiol. Rev. 18, 301–317.

Ferenci, T., 1999a. Growth of bacterial cultures' 50 years on: towards an uncertainty principle instead of constants in bacterial growth kinetics. Res. Microbiol. 150 (7), 431–438.

Ferenci, T., 1999b. Regulation by nutrient limitation. Curr. Opin. Microbiol. 22 (2), 208–213.

Von Forster, H., 1959. Some Remarks on Changing Populations. Grune & Stratton, pp. 382.

Fredrickson, A.G., Tsuchiya, H.M., 1963. Continuous propagation of microorganisms. AIChE J. 9 (4), 459–468.

Guillou, V., Plourde-Owobi, L., Parrou, J.-L., Goma, G., François, J., 2004. Role of reserve carbohydrates in the growth dynamics of *Saccharomyces cerevisiae*. FEMS Yeast Res. 4 (September (8)), 773–787.

Hatzis, C., Srienc, F., Fredrickson, A.G., 1995. Multistaged corpuscular models of microbial growth: Monte Carlo simulations. BioSystems 36, 19–35.

Joseph, H., 2005. Approximative kinetic formats used in metabolic network modeling. Biotechnol. Bioeng. 91 (September (5)), 534–545.

Kätterer, L., Allemann, H., Käppeli, O., Fiechter, A., 1986. Transient responses of continuously growing yeast cultures to dilution rate shifts: a sensitive means to analyze biology and the performance of equipment. Biotechnol. Bioeng. 28 (1), 146–150.

Kovàrovà-Kovar, K., Egli, T., 1998. Growth kinetics of suspended microbial cells: from single-substrate-controlled growth to mixed-substrate kinetics. Microbiol. Mol. Biol. Rev. 62, 646–666.

Lara, A.R., Taymaz-Nikerel, H., Mashego, M.R., van Gulik, W.M., Heijnen, J.J., Ramírez, O.T., van Winden, W.A., 2009. Fast dynamic response of the fermentative metabolism of *Escherichia coli* to aerobic and anaerobic glucose pulses. Biotechnol. Bioeng. 104 (6), 1153–1161.

Lebowitz, J.L., Rubinow, S.I., 1974. A theory for the age and generation time distribution of a microbial population. J. Math. Biol. 103, 17–36.

Mantzaris, N.V., 2005. A cell population balance model describing positive feedback loop expression dynamics. Comput. Chem. Eng. 29, 897–909.

Mantzatis, N.V., 2006. Stochastic and deterministic simulation of heterogeneous cell population dynamics. J. Theor. Biol. 241, 690–706.

Mischler, S., Perthame, B., Ryzhik, L., 2004. Stability in a nonlinear population maturation model. Math. Models Methods Appl. Sci. 12 (12), 1751.

Morchain, J., Fonade, C., 2009. A structured model for the simulation of bioreactors under transient conditions. AIChE J. 55 (11), 2973–2984.

Morchain, J., Gabelle, J.-C., Cockx, A., 2013. Coupling of biokinetic and population balance models to account for biological heterogeneity in bioreactors. AIChE J. 59 (2), 369–379.
Morchain, J., Pigou, M., Lebaz, N., 2017. A population balance model for bioreactors combining interdivision time distributions and micromixing concepts. Biochem. Eng. J. 126 (October), 135–145.
Morchain, J., 2017. Bioreactor Modeling. Interactions between Hydrodynamics and Biology. ISTE Press Ltd/Elsevier Ltd, London/Oxford.
Natarajan, A., Srienc, F., 2000. Glucose uptake rates of single *E. coli* cells grown in glucose-limited chemostat cultures. J. Microbiol. Methods 42 (1), 87–96.
Neubauer, P., Häggström, L., Enfors, S.-O., 1995. Influence of substrate oscillations on acetate formation and growth yield in *Escherichia coli* glucose limited fed-batch cultivations. Biotechnol. Bioeng. 47 (2), 139–146.
Nobs, J.-B., Maerkl, S.J., 2014. Long-term single cell analysis of *S. pombe* on a microfluidic microchemostat array. PLOS ONE 9 (4), 1–11.
Patarinska, T., Dochain, D., Agathos, S.N., Ganovski, L., 2000. Modelling of continuous microbial cultivation taking into account the memory effects. Bioprocess Biosyst. Eng. 22 (6), 517–527.
Perret, J., 1960. A New kinetic model of growing bacteria population. J. Gen. Microbiol. 241, 589–617.
Perthame, B., 2007. Transport Equations in Biology. Springer, birkhäuser verlag edition.
Pigou, M., Morchain, J., 2015. Investigating the interactions between physical and biological heterogeneities in bioreactors using compartment, population balance and metabolic models. Chem. Eng. Sci. 126 (0), 267–282.
Robert, L., Hoffmann, M., Krell, N., Aymerich, S., Robert, J., Doumic, M., 2014. Division in *Escherichia coli* is triggered by a size-sensing rather than a timing mechanism. BMC Biol. 12 (17).
Rotenberg, M., 1977. Selective synchrony of cells of differing cycle times. J. Theor. Biol. 66, 389–398.
Rotenberg, M., 1983. Transport theory for growing cell populations. J. Theor. Biol. 103, 181–199.
Shah, B.H., Borwanker, J.D., Ramkrishna, D., 1976. Monte Carlo simulation of microbial population growth. Math. Biosci. 31, 1–23.
Silveston, P.L., Budman, H., Jervis, E., 2008. Forced modulation of biological processes: a review. Chem. Eng. Sci. 63 (20), 5089–5105.
Smoluchowski, M., 1916. Drei Vorträge über Diffusion, Brownsche Molekularbewegung und Koagulation von Kolloidteilchen. Phys. Z. 17, 557–571, 585-599.
Stamatakis, M., Zygourakis, K., 2010. A mathematical and computational approach for integrating the major sources of cell population heterogeneity. J. Theor. Biol. 266, 41–61.
Subramanian, G., Ramkrishna, D., Fredrickson, A.G., Tsuchiya, H.M., 1970. On the mass distribution model for microbial cell populations. Bull. Math. Biophys. 32, 521–537.
Sunya, S., Delvigne, F., Uribelarrea, J.-L., Molina-Jouve, C., Gorret, N., 2012. Comparison of the transient responses of *Escherichia coli* to a glucose pulse of various intensities. Appl. Microbiol. Biotechnol. 95, 1021–1034.
Trucco, E., 1965. Mathematical models for cellular systems. The Von Foerster equation. Bull. Math. Biophys. 27, 285–304.
Yasuda, K., 2011. Algebraic and geometric understanding of cells: epigenetic inheritance of phenotypes between generations. High Resolut. Microb. Single Cell Anal. 124, 55–81.